SERBIAN JOURNAL OF ELECTRICAL ENGINEERING
Vol. 23, No. 2, June 2026, 183-202

UDC: 621.317.43 **DOI: https://doi.org/10.2298/SJEE2602183H**

Original scientific paper

Time-Domain Iron Loss Estimation Using the Parametric Magneto Dynamic Model: Discretisation Sensitivity and a Skin-Depth-Based Heuristic

Timo Hörmann[1], Ermin Rahmanovic[2], Danilo Gartner Aurich[1], Martin Petrun[2], Simon Steentjes[1]

Abstract: This paper utilizes the Parametric Magneto-Dynamic (PMD) model, enhanced with an inverse hysteresis formulation, to estimate iron losses in the time domain under arbitrary excitation waveforms. The proposed PMD model reproduces the intricate magnetization dynamics of advanced steel grades, facilitating a systematic investigation into how metallurgical and geometric material properties - such as lamination thickness, alloy composition, and grain morphology - influence the required spatial and temporal discretisation for accurate loss estimation. The paper evaluates the consequences of discretisation parameters in the PMD model on both the accuracy of the iron loss prediction accuracy and computational overhead. The findings establish rigorous guidelines on the required discretisation schemes for purely sinusoidal excitation and for non-sinusoidal regimes with significant harmonic content across a broad frequency spectrum.

Keywords: Iron loss calculation, Dynamic iron loss, Hysteresis, Electrical steel sheet, Parametric Magneto-Dynamic model.

1 Introduction

Precise characterization of iron losses remains a critical aspect of designing high-performance electric drives [1]. Traditional analytical models, predicated on

[1]Institute of Electrical Machines, RWTH Aachen University, Aachen, Germany
timo.hoermann@iem.rwth-aachen.de, https://orcid.org/0009-0007-2699-2991
danilo.aurich@iem.rwth-aachen.de, https://orcid.org/0009-0000-3360-2102
simon.steentjes@iem.rwth-aachen.de, https://orcid.org/0000-0002-3346-4560
[2]Faculty of Electrical Engineering and Computer Science, Institute of Electrical Power Engineering, University of Maribor, Maribor, Slovenia
ermin.rahmanovic@um.si, https://orcid.org/0009-0007-6956-6634
martin.petrun@um.si, https://orcid.org/0000-0001-9134-5802

Colour versions of the one or more of the figures in this paper are available online at https://sjee.ftn.kg.ac.rs statistical loss separation and sinusoidal excitation, often employ frequency-domain techniques, such as the linear superposition of harmonic components [2], which necessitate extensive measurement data. Approaches like [3] address non-sinusoidal excitation by decoupling major and minor hysteresis loops and utilizing DC-biased sinusoidal measurements to extract material-dependent parameters for frameworks such as Bertotti's [4]. In particular, [3] provides a method for estimating iron losses that leverages these DC-biased parameters to evaluate and accumulate the individual contributions of each minor loop within a general hysteresis waveform. However, these frequency-domain methods are fundamentally unsuitable for real-time and time-domain applications. Meanwhile, advancements in electrical steel – characterized by thinner laminations (≤0.27 mm), higher silicon content, and coarse grain structures - introduce complexities in field distribution that are not adequately captured by conventional models.

Several studies have attempted to circumvent this problem by proposing time-domain models for calculating iron losses under arbitrary excitation conditions [5]. One such example is the Loss Surface (LS) model [6], where iron losses are determined based on surfaces interpolated from measurements performed under purely sinusoidal excitation [7, 8]. An arbitrary hysteresis loop is then reconstructed by interpolating the surface obtained for different peak flux densities and frequencies, typically assuming symmetric excitation conditions. The primary limitation of this method is the requirement for an extensive experimental dataset to construct the surface. Moreover, the LS model remains phenomenological and does not explicitly account for the underlying physical loss mechanisms.

This study addresses these limitations by employing a physically based formulation, namely the Parametric Magneto-Dynamic (PMD) model [9] in combination with an inverse hysteresis model to facilitate accurate, time-domain iron loss estimation under arbitrary excitation conditions. Unlike preceding models, the PMD framework inherently supports time-domain analysis and permits the direct incorporation of nonlinear magnetization dynamics influenced by material microstructure [10, 11].

Due to this nonlinear constitutive behaviour, the magnetic permeability becomes state-dependent, which governs the diffusion of electromagnetic fields within the material. Consequently, the field distribution across the lamination thickness may deviate significantly from classical skin-effect predictions derived under linear material assumptions. Therefore, in numerical implementations of the PMD model, the discretisation density across the thickness of a sheet material must be chosen based on both the skin depth and the transient excitation dynamics. As skin depth governs flux penetration depth, a practical heuristic is to assign one slice per skin depth [9] to ensure sufficient spatial simulation resolution.

This work systematically analyzes the influence of sheet discretisation, specifically, the selected number of slices on the accuracy and computational efficiency of the PMD model for an iron-silicon electrical sheet. The analysis was performed under purely sinusoidal excitations as well as non-sinusoidal waveforms containing harmonic components. Multiple excitation frequencies were considered, specifically 20 Hz, 100 Hz, 200 Hz, 400 Hz, 800 Hz and 1000 Hz. The non-sinusoidal cases consisted of fundamental frequencies of 100 Hz and 500 Hz with a third harmonic. In addition, this work introduces a guideline for determining the optimal number of slices based on the classical skin depth for both excitation cases.

The paper is structured as follows: Section 2 outlines the PMD model and the associated static hysteresis model is presented. Section 3 details the experimental material, the measurement protocols, and the methodology for iron loss computation. Subsequently, Section 4 presents and discusses the influence of discretisation on accuracy and simulation time.

2 Material Modelling Considering Major and Minor Loops

2.1 Parametric magneto-dynamic model

Since iron losses comprise both hysteresis and eddy current losses, it is essential to account for both, in order to accurately estimate the total iron losses in electrical sheets. The PMD model [9] is based on Maxwell's equations and enhances computational efficiency by segmenting electrical steel sheets into thinner slices and applying a piecewise approximation of magnetic quantities. This approach simplifies calculation while allowing for the integration of various static hysteresis models. The PMD model was introduced in [12], its ability to handle arbitrary excitations was demonstrated in [10] and [11]. The PMD model, used in this study, can be expressed as

$$\boldsymbol{H}(\boldsymbol{B}) = \boldsymbol{H}_{\text{sur}} - \boldsymbol{K}\frac{\mathrm{d}\boldsymbol{B}}{\mathrm{d}t}, \tag{1}$$

where $\boldsymbol{H}(\boldsymbol{B})$ represents the averaged magnetic field strength in every slice, which depends on the flux density of the corresponding slice, $\boldsymbol{H}(\boldsymbol{B}) = \left[H_1(B_1), H_2(B_2), \ldots, H_{\text{s}}(B_{\text{s}})\right]^{\text{T}}$.

Here $\boldsymbol{H}_{\text{sur}} = \left[H_{\text{sur}}, H_{\text{sur}}, \ldots, H_{\text{sur}}\right]^{\text{T}}$ represents the applied field strength extended uniformly to each slice, matrix $\boldsymbol{K}$ in (1), couples the slices in the form of

$$\boldsymbol{K} = \sigma b_{\mathrm{s}}^2 \begin{bmatrix} (N_{\mathrm{s}}-1)+\frac{1}{3} & (N_{\mathrm{s}}-2)+\frac{1}{2} & \cdots & \frac{1}{2} \\ (N_{\mathrm{s}}-2)+\frac{1}{3} & (N_{\mathrm{s}}-2)+\frac{1}{2} & \cdots & \frac{1}{2} \\ \vdots & \vdots & \ddots & \vdots \\ \frac{1}{2} & \frac{1}{2} & \cdots & \frac{1}{3} \end{bmatrix} \tag{2}$$

with σ as the electrical conductivity and b_{s} as the thickness of each slice b_{s} is calculated as

$$b_{\mathrm{s}} = \frac{b}{2N_{\mathrm{s}}}. \tag{3}$$

The total thickness of the sheet is denoted by b. The individual slices are indexed by $s \in N$, with $1 \leq s \leq N_s$, where N_s denotes the total number of slices in the simulated half of the lamination. To ensure that the simulation results accurately represent the behaviour of the entire sheet, a symmetric extension is applied during the evaluation phase. This process involves mirroring the computed data across the sheet's mid-plane and appropriately scaling the results to represent the full thickness b. In this context, the first slice ($s = 1$) corresponds to the mid-plane of the sheet, while the last slice $s = N_s$ represents the outermost layer of the simulated half. The selection of N_s is pivotal for achieving high accuracy; however, increasing N_s commensurately elevates computational complexity. Therefore, an optimal balance between accuracy and computational efficiency must be struck. While [13] proposed a non-uniform discretisation to account for the rapid field gradients at the surface caused by skin effect, the present work utilizes an implementation with constant slice thickness. The discretisation principle is schematically illustrated in Fig. 1 using four slices, $N_s = 4$. The sheet's thickness is represented by b, and as Fig. 1 depicts, the innermost slice is $s = 1$ and the outermost is $s = 4$. By applying the PMD model, the assumption is made that the width $w \gg b$ and the length $l \gg b$.

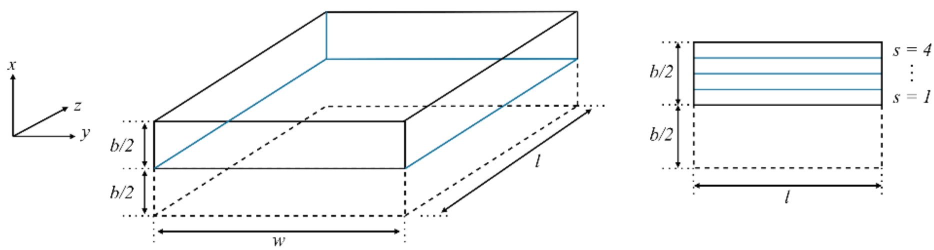

Fig. 1 – *Schematic view of the discretisation of the PMD model.*

2.2 Static hysteresis model

To accurately replicate hysteresis behaviour under arbitrary excitation with the PMD model, a well-suited static inverse hysteresis model is essential. Numerous hysteresis models have been developed, each with its own advantages and disadvantages, which can be found in [5]. After comparing the accuracy of several history-independent hysteresis models [14], the Tellinen (TLN) model [15] was chosen. The TLN model stands out for its ease of implementation and its ability to effectively reproduce symmetric loops of varying amplitudes using standard measurements. The model is implemented using two ordinary differential equations (ODEs):

$$\frac{\mathrm{d}H}{\mathrm{d}t}=\frac{1}{\mu_0+\dfrac{B^-_{\text{major}}(H)-B}{B^-_{\text{major}}(H)-B^+_{\text{major}}(H)}\left(\dfrac{\mathrm{d}B^+_{\text{major}}(H)}{\mathrm{d}H}-\mu_0\right)}\frac{\mathrm{d}B}{\mathrm{d}t},\quad \frac{\mathrm{d}B}{\mathrm{d}t}>0, \tag{4}$$

$$\frac{\mathrm{d}H}{\mathrm{d}t}=\frac{1}{\mu_0+\dfrac{B-B^+_{\text{major}}(H)}{B^-_{\text{major}}(H)-B^+_{\text{major}}(H)}\left(\dfrac{\mathrm{d}B^-_{\text{major}}(H)}{\mathrm{d}H}-\mu_0\right)}\frac{\mathrm{d}B}{\mathrm{d}t},\quad \frac{\mathrm{d}B}{\mathrm{d}t}<0, \tag{5}$$

where B^+_{major} describes the ascending and B^-_{major} the descending branch of the quasi-static BH loop of the measured material. $\mathrm{d}B^{+,-}_{\text{major}}/\mathrm{d}H$ denotes the permeability of the major loop and μ_0 the magnetic permeability constant. The variable B is the flux density. Depending on the sign of $\mathrm{d}B/\mathrm{d}t$ the model switches between the two ODEs. In this study, the TLN model was identified using a major loop measured at 10 Hz with a peak flux density of $B_{\text{sat}}=1.5\,\text{T}$.

3 Methodology

3.1 Material specification and measurement setup

Measurements, simulations, and analyses were performed on a $3.2\,\text{wt\%}$ non-grain-oriented electrical steel with a thickness of $b=0.3\,\text{mm}$ and dimensions of length $l=120\,\text{mm}$ and width $w=120\,\text{mm}$. The electrical conductivity σ, listed in **Table 1**, was determined by the four-point method.

The magnetic characterization required for parameterizing the TLN model and validating the PMD model were performed using a Single Sheet Tester (SST). As discussed in Section 2.2, the TLN model was parameterized using the measured major hysteresis loop, partially shown in Fig. 2a, which serves as a look-up table embedded in the model. The parametrization of $\mathrm{d}B/\mathrm{d}H$ is simply done by differentiating the major loop. Fig. 2b shows the relative permeability μ_r, which is calculated from $\mathrm{d}B/\mathrm{d}H$ and normalized by μ_0.

Table 1
Material parameters of the investigated material M280-30AP.

Density ρ	$7.6\ \mathrm{g/cm^3}$
Sample length l	120 mm
Sample width w	120 mm
Sample thickness b	0.3 mm
Electrical conductivity σ	1.8 MS/m

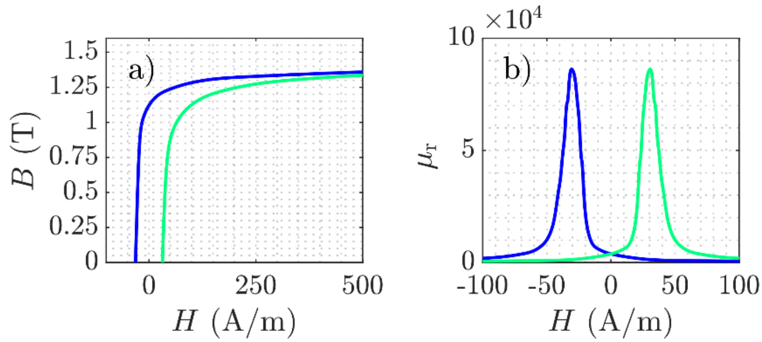

Fig. 2 – *Measured* (a) *static hysteresis loop of the electrical steel sheet used in this study and* (b) *relative permeability* μ_r *derived from the measured major loop.*

The experimental scenarios listed in **Table 2** were conducted and evaluated though both measurements and simulations. Different numbers of slices N_s were used to demonstrate the model's ability to process arbitrary excitations – in particular, purely sinusoidal and non-sinusoidal signals with harmonic components – using the time-based PMD model. The respective measurements are summarized in **Table 2**, where f_1 and f_3 denote the fundamental frequency and the frequency of the third harmonic of the excitation, respectively. B_1 and B_3 represent the corresponding flux densities. The third harmonic exhibits no phase shift.

The time-dependent excitation H of a major loop (case 2), as well as that of a major loop containing minor loops (case 7), is illustrated in Fig. 3a. The corresponding simulated time-domain waveforms of the flux density B. are presented in Fig. 3b, while Fig. 3c shows the resulting hysteresis curves. It can be observed that, at the same fundamental frequency, the presence of the harmonic component leads to a significant widening of the hysteresis curve. It should be emphasized that the results presented in Fig. 3 are obtained from simulations. The input of the PMD model H_{sur} is shown in Fig. 3a as H, while the resulting B is the output of the PMD model.

Table 2
Tested excitation cases with corresponding frequencies and flux densities.

Case	Excitation
1-6	$f_1 = \{20, 100, 200, 400, 800, 1000\}$ Hz, $B_1 = 1.2$ T
7	$f_1 = 100$ Hz, $B_1 = 1.2$ T; $f_3 = 300$ Hz, $B_3 = 0.5$ T
8	$f_1 = 500$ Hz, $B_1 = 1.2$ T; $f_3 = 1500$ Hz, $B_3 = 0.5$ T

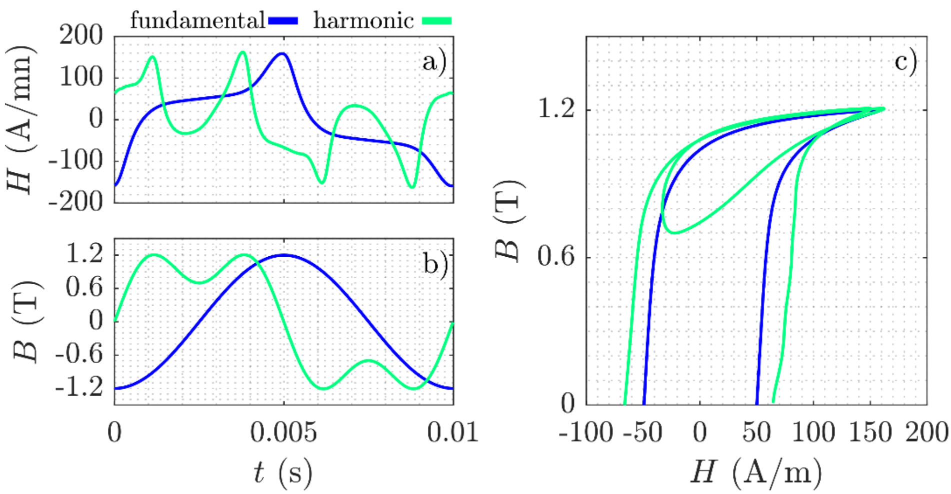

Fig. 3 – Waveforms of (a) *time-dependent excitation H*, (b) *resulting simulated flux densities B, and* (c) *corresponding hysteresis curves.*

3.2 Iron loss calculation

Iron losses play a significant role in the overall efficiency of electrical machines and the accurate calculation of these losses is essential for design optimization and effective thermal management. Various methods exist for determining iron losses, depending on the type of excitation and the available data [2, 3, 16, 17].

Thermodynamically, the specific hysteresis power loss P_{c}, is defined as the energy density enclosed by the *BH* hysteresis loop over a magnetization cycle. When normalized by mass and frequency, the loss is determined by:

$$P_{\mathrm{c}} = \frac{f_{\mathrm{c}}}{\rho}\oint H\,\mathrm{d}B\,, \tag{6}$$

where P_{c} denotes the power loss due to hysteresis, f_{c} is the frequency, t_{c} the cycle time of the magnetization cycle, and ρ denotes the density of the corresponding material. The classical Bertotti formula [4] describes the total iron losses as the sum of hysteresis, eddy current, and excess losses:

$$P_{\mathrm{B}} = c_{\mathrm{hyst}} B^{\alpha} f + c_{\mathrm{eddy}} B^2 f^2 + c_{\mathrm{excess}} B^{1.5} f^{1.5}\,, \tag{7}$$

where α, c_{hyst}, c_{eddy}, and c_{excess} are material-specific parameters. The coefficient for eddy current losses can be determined by [18]:

$$c_{\mathrm{eddy}} = \frac{\pi^2 b^2 \sigma}{6\rho}. \tag{8}$$

The remaining parameters must be identified through experiments and subsequent parameter fitting.

However, since the classical Bertotti formulation is primarily intended for sinusoidal excitations, it lacks accuracy under arbitrary waveforms. To remedy this, a loss computation approach tailored to the PMD model was adopted [9]. This method obviates the need for extensive parameter fitting by relying on available material data. The slice-wise eddy current power loss is calculated by integrating the squared rate of change of flux density across each slice (9), and the total loss is obtained by aggregating these contributions.

$$P_{\mathrm{ec,s}} = f_{\mathrm{c}} \int_{t_{\mathrm{s}}}^{t_{\mathrm{e}}} \left[\frac{\sigma b_{\mathrm{s}}^2}{N_{\mathrm{s}}\rho} \left(\left(\sum_{i=1}^{s-1} \frac{\mathrm{d}B_i}{\mathrm{d}t} \right)^2 + \left(\sum_{i=1}^{s-1} \frac{\mathrm{d}B_i}{\mathrm{d}t} \right) \frac{\mathrm{d}B_{\mathrm{s}}}{\mathrm{d}t} + \frac{1}{3} \left(\frac{\mathrm{d}B_{\mathrm{s}}}{\mathrm{d}t} \right)^2 \right) \right] \mathrm{d}t\,. \tag{9}$$

In (9), t_{s} and t_{e} denote the start and end times of the magnetization cycle, respectively, and B_{s} represents the flux density in the respective slice s. To obtain the total eddy current-induced iron loss, P_{ec}, the slice-wise contributions from (9) must be summed over all slices:

$$P_{\mathrm{ec}} = \sum_{i=1}^{N_{\mathrm{s}}} P_{\mathrm{ec},i}\,. \tag{10}$$

The hysteresis losses per slice, $P_{\mathrm{hyst,s}}$, are calculated by:

$$P_{\mathrm{hyst,s}} = f_{\mathrm{c}} \int_{t_{\mathrm{s}}}^{t_{\mathrm{e}}} \frac{1}{N_{\mathrm{s}}\rho} H_{\mathrm{s}} \frac{\mathrm{d}B_{\mathrm{s}}}{\mathrm{d}t} \mathrm{d}t. \tag{11}$$

To obtain the total hysteresis loss, P_{hyst}, the individual slice contributions must be summed in the same manner as in (10). To compare the measured iron losses with those predicted by the PMD model, the total power loss per cycle, $P_{c,n}$, is determined by summing (10) and (11):

$$P_{c,n} = P_{ec} + P_{hyst}. \tag{12}$$

In the present study, the excess loss term in Bertotti's formulation (7) (third term on the right-hand side) is omitted. For the investigated material, the hysteresis and eddy current components already provide a sufficiently accurate prediction of the iron losses. This may be attributed to the spatial resolution of the slices, which captures non-linear field distributions that are typically approximated by the excess loss term in analytical loss-separation models. To validate the simulation results, both absolute and relative errors are used. The absolute error is defined as

$$\epsilon_a = P_m - P_{c,n} \tag{13}$$

and the relative error as

$$\epsilon_r = \frac{P_m - P_{c,n}}{P_m} 100\,\%. \tag{14}$$

The absolute error (13) and relative error (14), alongside (10) and (11), are used as metrics in the present study to assess the accuracy of the PMD model under various excitation conditions.

4 Results

Since this study investigates the influence of slice count on simulation time, all simulations were conducted on identical hardware to ensure consistent conditions. Both the PMD model and the implemented TLN model were developed in MATLAB/Simulink. Consequently, the choice of the numerical solver and its settings directly affect the simulation results.

In this work, the built-in MATLAB solver ode23tb was employed with a variable step size, which was limited to a maximum value of $1 \cdot 10^{-3}$ s. Both the relative and absolute error tolerances were set to $5 \cdot 10^{-8}$, ensuring a balance between accuracy and computational efficiency.

Each simulation was run for 10 consecutive cycles, as the PMD model requires several cycles–depending on the material properties–to reach a stable steady-state. For analytic purposes, only the results from the last cycle were considered.

4.1 Spatial behaviour

As illustrated in Fig. 4a, the magnetic field distribution within the sheet is already non-uniform at 100 Hz and exhibits a phase lag, as the inner slices reach the applied flux density later in time. This behaviour highlights the necessity of discretizing the electrical steel sheet–an approach inherently provided by the

PMD model. The following time-dependent figures are normalized by the magnetization cycle time t_c, whereas the spatially dependent figures are normalized by the sheets thickness b.

The simulation results also demonstrate field attenuation within the material: the innermost slice (depicted in vibrant blue) exhibits significantly lower flux density compared to the outermost slice (shown in light green) at $t/t_c = 0.25$. Fig. 4b and d shows the flux density averaged across all slices as a function of slice position. As expected, the field distribution remains nearly homogeneous at $t/t_c = 0.0$ and $t/t_c = 0.5$, while the most significant variation across the sheet occurs around $t/t_c \approx 0.2$.

Since (7) assumes a homogeneous field distribution within the material [4], it does not accurately capture the non-uniform field behaviour illustrated in Fig. 4, resulting in imprecise iron loss estimations. Unlike the approach in [9], which specifically addresses field distribution under viscous magnetic conditions, this study does not consider magnetic viscosity.

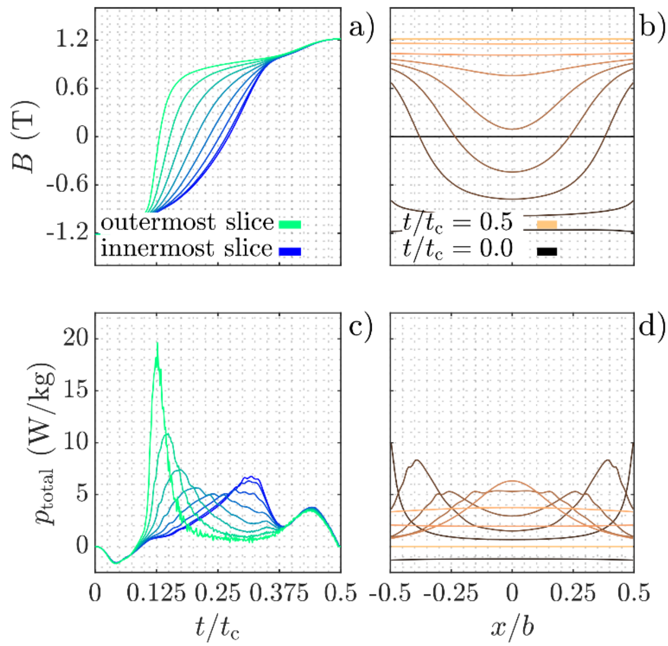

Fig. 4 – Variation of (a) *B over time*, (b) *B across sheet position,* (c) p_{total} *over time and* (d) p_{total} *over slice position, at* 100 Hz *and peak B of* 1.2 T.

In Fig. 5, the field distribution at 400 Hz is shown. At this higher frequency, the disparity between the innermost and outermost slices increases further, reinforcing the importance of spatially resolved modelling for accurate representation of the internal field behaviour. Additionally, a transient power peak occurs due to high $\mathrm{d}B/\mathrm{d}t$ as shown in Fig. 5c.

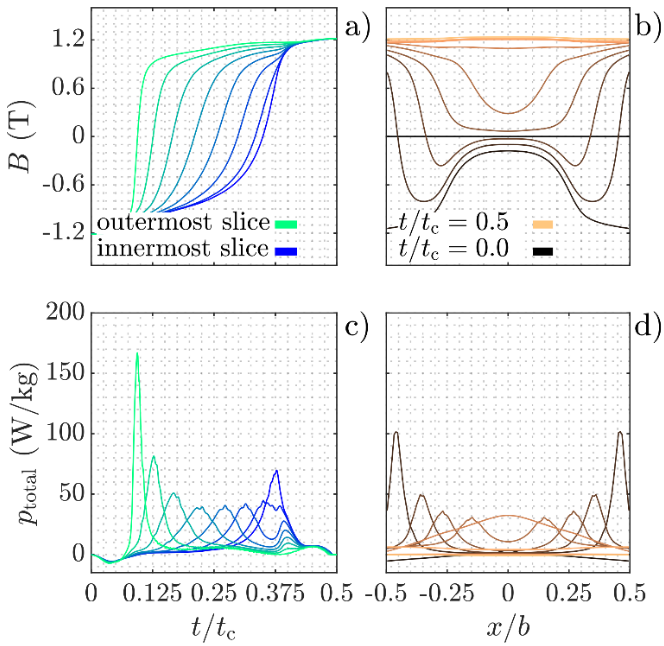

Fig. 5 – Variation of (a) *B over time*, (b) *B across sheet position,* (c) p_{total} *over time and* (d) p_{total} *over slice position, at* 400 Hz *and peak B of* 1.2 T.

At higher excitation frequencies, such as $1000\,\text{Hz}$, the variation in field distribution becomes even more pronounced, as shown in Fig. 6. The outermost slice exhibits a behaviour characteristic of the well-known hysteresis loop, whereas the innermost slice shows a smoother and more delayed response over time. The outermost slice exhibits high power over a short duration (up to $650\,\text{W/kg}$), whereas the inner slices exhibit much lower power levels ($\approx 250\,\text{W/kg}$). The instantaneous power of the slices exhibits wave-like behaviour, with the peak propagating from one slice to the next toward the interior of the sheet with a time delay. This phenomenon also observable at lower frequencies, but it is less distinct.

In Fig. 7, a non-sinusoidal excitation is applied, consisting of a fundamental component with an amplitude of 1.2 T at 100 Hz and a third-order harmonic with an amplitude of 0.5 T. A phase lag is observed in the inner slices. At $t/t_c = 0.0$, the flux density distribution resembles that of a pure sinusoidal excitation. However, when the harmonic component becomes significant ($t/t_c \approx 0.2$), the flux density in the inner slices decreases, even falling below the excitation level.

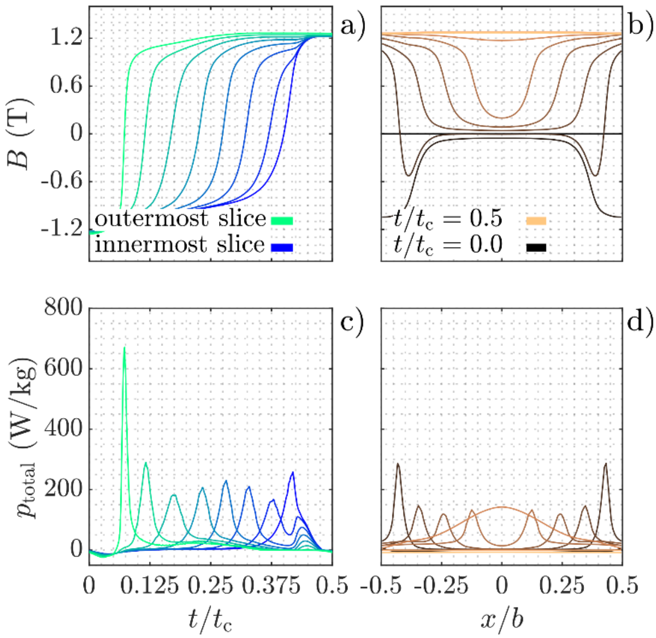

Fig. 6 – Variation of (a) B *over time*, (b) B *across sheet position,* (c) p_{total} *over time and* (d) p_{total} *over slice position, at* 1000 Hz *and peak* B *of* 1.2 T.

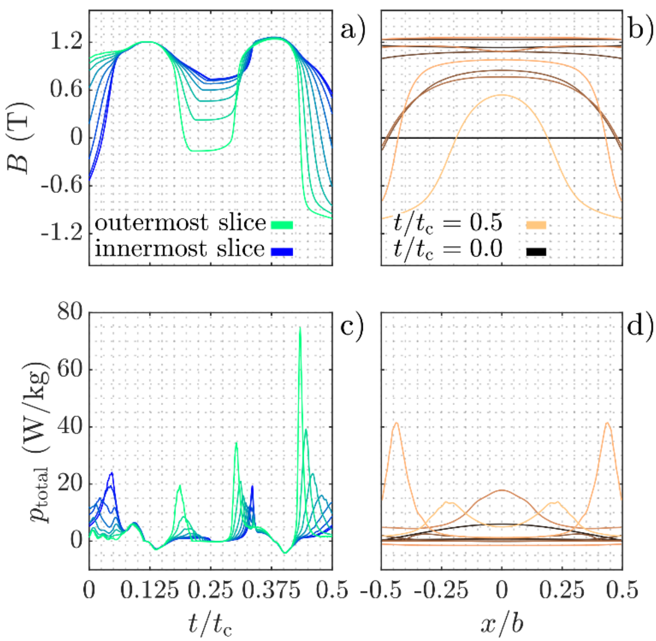

Fig. 7 – Variation of (a) B *over time*, (b) B *across sheet position,* (c) p_{total} *over time and* (d) p_{total} *over slice position, at* 100 Hz *and peak* B *of* 1.2 T *and harmonic component at* 300 Hz *with amplitude of* 0.5 T.

By increasing the fundamental frequency from 100 Hz to 500 Hz, the outermost slice exhibits a flux density of approximately $-1.0\ \mathrm{T}$, at $t/t_c \approx 0.2$ indicating that the harmonic component of the excitation causes a flux inversion in the outer regions of the electrical steel sheets, as shown in Fig. 8.

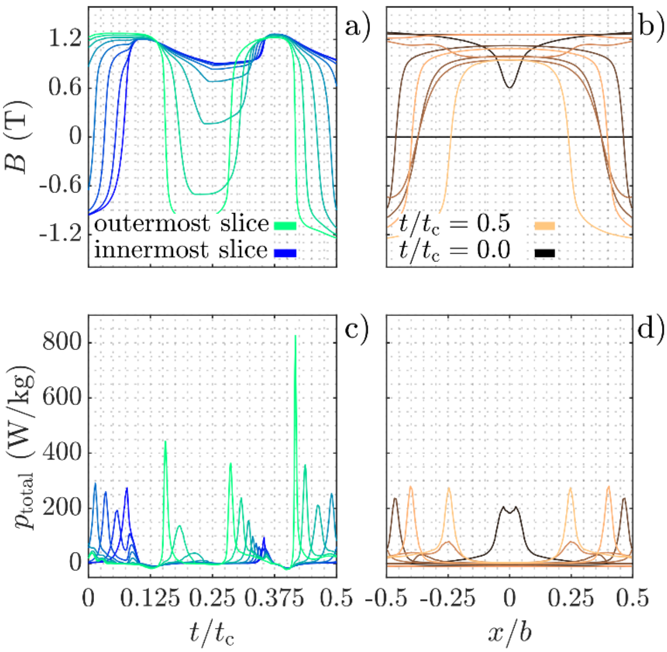

Fig. 8 – Variation of (a) *B over time*, (b) *B across sheet position,* (c) p_{total} *over time and* (d) p_{total} *over slice position, at* 500 Hz *and peak B of* 1.2 T *and harmonic component at* 1500 Hz *with amplitude of* 0.5 T.

4.2 Influence of discretisation on accuracy and simulation time

As shown in Section 4.1, selecting an appropriate number of slices is essential to accurately capture the inhomogeneous flux distribution caused by eddy currents. First, the influence of the slice count N_s on the simulation time t_{sim} is investigated. As illustrated in Fig. 9, the simulation time decreases with increasing frequency. At frequencies above 100 Hz, the simulation time reliably converges to a frequency-independent value across all tested values.

Furthermore, depending on the excitation frequency, increasing the number of slices N_s does not necessarily lead to improved accuracy. This suggests that, beyond a certain point, additional discretisation does not yield greater accuracy.

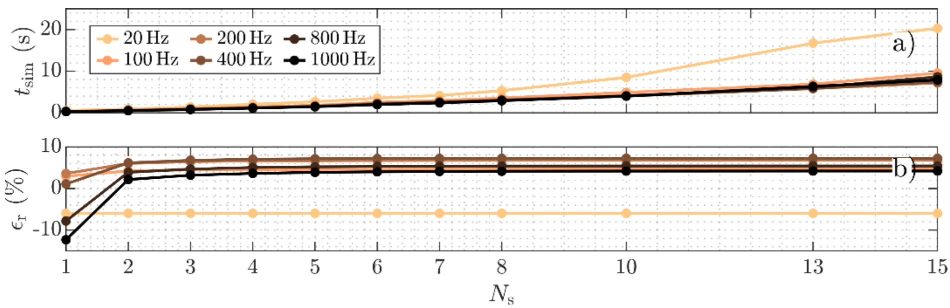

Fig. 9 – *Variation of* (a) *simulation time t_{sim} and*
(b) *relative error ε_r with N_s for fundamental excitations.*

This is further confirmed by the simulation results under harmonic excitation, as shown in Fig. 10. The simulation time is approximately $t_{sim} = 20\,\mathrm{s}$, which is slightly higher compared to the simulation with a 100 Hz fundamental excitation. The relative error ϵ_r converges for the 500 Hz simulation when the number of slices reaches $N_s = 8$.

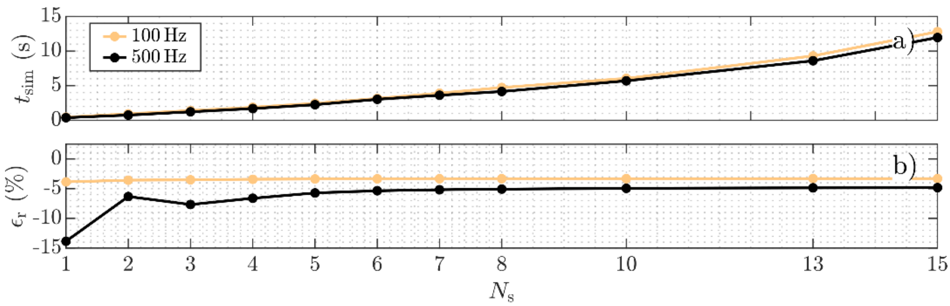

Fig. 10 – *Variation of* (a) *simulation time t_{sim} and*
(b) *relative error ε_r with N_s for harmonic excitations.*

Fig. 11 provides an overview of the power losses due to eddy currents (P_{ec}), hysteresis losses (P_{hyst}), and the total losses (P_{total}). Additionally, the absolute error (ϵ_a) and the relative error (ϵ_r) are shown. Figs. 11a, 11c, 11e, 11g, and 11i illustrate the frequency dependency, while Figs. 11b, 11d, 11f, 11h, and 11j display the slice-count-dependent values. This enables a more detailed analysis of the model behaviour. The red dots in Figs. 11e and 11f indicate the total measured iron losses from the experiments.

Fig. 11a confirms the expected quadratic increase of eddy current losses with frequency, while the hysteresis losses P_{hyst} increase approximately linearly. Furthermore, it can be observed that the hysteresis losses are consistently lower than the eddy current losses. The total losses P_{total} show good overall agreement with the measured losses P_{m}.

As illustrated in Fig. 11i, the PMD model tends to overestimate losses at low frequencies and underestimate them at mid-range frequencies. This deviation may result from the absence of additional effects–such as viscous fields–and the fact that the TLN model parametrization was based on measurements at 10 Hz, which is not a truly static measurement. At higher frequencies, the estimation becomes more accurate again, except when only a single slice ($N_{\text{s}} = 1$) is used for discretisation.

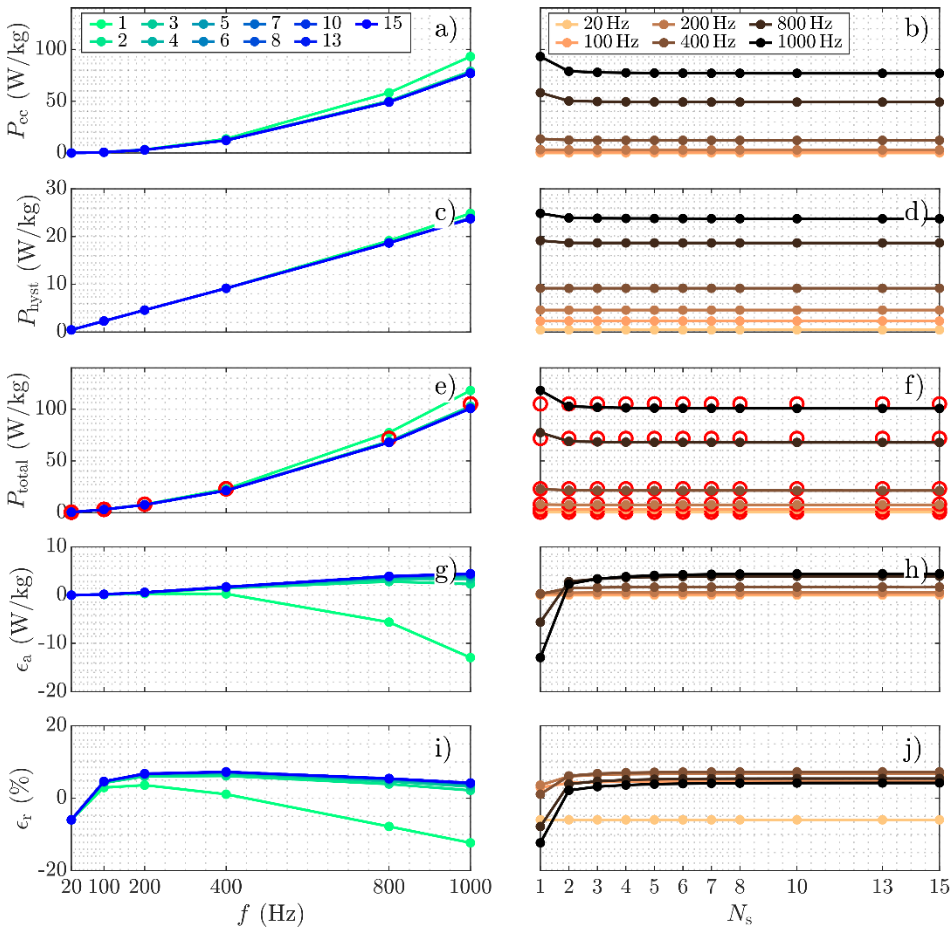

Fig. 11 – *Frequency- and slice-count-dependent power loss components with relative and absolute errors at fundamental excitation:* (a, b) *eddy current losses,* (c, d) *hysteresis losses,* (e, f) *total losses,* (g, h) *absolute error and* (i, j) *relative error.*

The simulation results for harmonic excitation are shown in Fig. 12. The red bars represent the measured total iron losses P_{m} at $f_1 = 100\,\mathrm{Hz}$ and $f_1 = 500\,\mathrm{Hz}$. As previously described, the excitation consists of a fundamental frequency component f_1 and a third-order harmonic. The amplitude of the fundamental component is set to 1.2 T, while the third harmonic is set to 0.5 T.

At $f_1 = 100\,\mathrm{Hz}$, the PMD model provides an accurate iron loss estimation with as few as $N_{\mathrm{s}} = 6$ slices. When using $N_{\mathrm{s}} = 10$, the model accurately replicates the magnetic behaviour across the sheet.

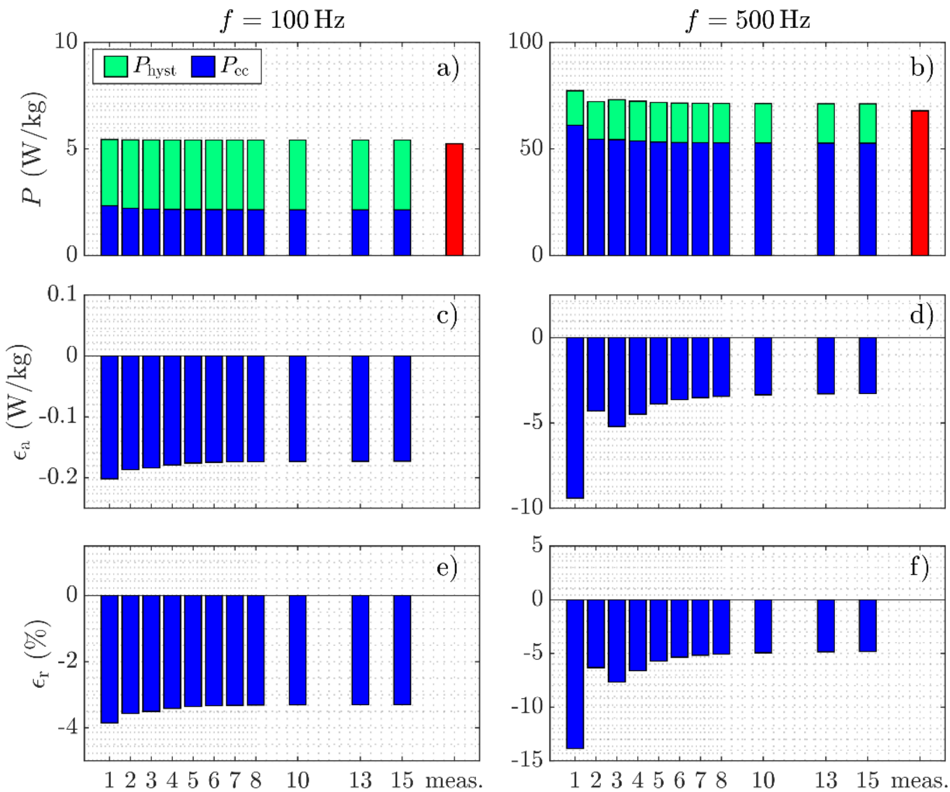

Fig. 12 – *Slice-count-dependent power loss components with relative and absolute errors at harmonic excitation:* (a, b) *combined eddy current and hysteresis losses,* (c, d) *absolute error and* (e, f) *relative error.*

The total power loss P_{total}, as well as the separated eddy current losses P_{ec} and hysteresis losses P_{hyst} as a function of the slice count N_{s}, are shown in Figs. 13a, 13b, and 13c. The red dots in Fig. 13c represent the experimentally measured losses. A relative error of only $5\,\%$ is achieved using the PMD model when the slice count reaches $N_s \geq 10$.

In comparison to Fig. 11, the PMD model tends to overestimate the losses under harmonic excitation.

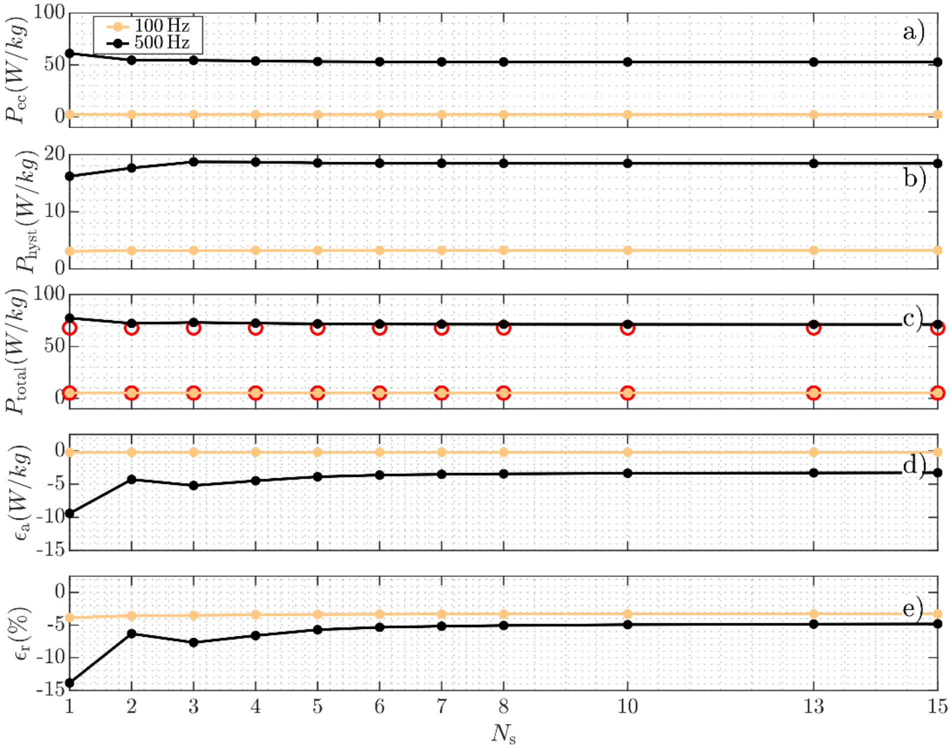

Fig. 13 – *Time-count-dependent power loss components with relative and absolute errors at harmonic excitation.*

4.3 Derivation of a skin-depth-based discretisation heuristic

Prior literature [9] has suggested a discretisation strategy where one slice is allocated per skin depth. While a single slice may be sufficient under quasi-static conditions or when the skin depth exceeds the laminate thickness, this assumption becomes untenable at frequencies as low as 100 Hz. For non-sinusoidal or high-frequency excitations, the assumption of homogeneity is categorically invalid, as shown in Figs. 4 – 8. Consequently, this work formulates a discretisation heuristic to estimate the minimum N_s required for high-fidelity modelling. The minimum skin depth δ_{min} is defined as

$$\delta_{\text{min}} = \sqrt{\frac{1}{\pi f_{\text{max}} \mu_0 \mu_{\text{r,max}} \sigma}}, \tag{1}$$

where f_{max} is the maximum significant frequency component and σ is the electrical conductivity. To ensure the heuristic remains conservative under highly non-linear conditions, $\mu_{\text{r,max}}$ is defined as the maximum relative differential permeability observed during the cycle:

$$\mu_{\text{r,max}} = \frac{1}{\mu_0} \max\left(\frac{\mathrm{d}B}{\mathrm{d}H}\right). \tag{2}$$

The required number of slices N_{s} is then computed via

$$N_{\text{s}} = \left\lceil \frac{b}{\delta_{\text{min}}} \right\rceil, \tag{3}$$

where the ceiling operator ensures that the discretisation captures the full extent of the field gradients. **Table 3** contrasts the analytically derived values with those determined graphically. The results confirm the robustness of the heuristic for both sinusoidal and harmonic-rich excitations.

Table 3

Calculated and graphically determined skin depths for the fundamental and harmonic frequencies, along with the corresponding number of slices N_{s}.

Sinusoidal excitation						
Excitation frequency [Hz]	20	100	200	400	800	1000
Calculated	1	3	4	5	8	8
Graphically determined	2	3	4	5	7	8

Harmonic excitation		
Maximum Excitation frequency [Hz]	300	1500
Calculated	6	10
Graphically determined	5	10

5 Conclusion

This paper examined the application of the PMD model coupled with the static hysteresis TLN model applied to a non-grain oriented electrical steel grade. The findings underscore the necessity of precisely quantifying both hysteresis and eddy current losses to enhance loss prediction in electrical machines. By incorporating the PMD model, the through-thickness magnetization dynamics are resolved, providing critical insights into flux density distribution and magnetodynamic effects.

The piecewise approximation inherent to the PMD model simplifies the numerical characterization of eddy currents while facilitating spatial resolution across the lamination. However, a trade-off arises between simulation accuracy and computational overhead, which is directly influenced by the chosen number of slices, i.e. the discretisation density. To mitigate this, a skin-depth-derived heuristic was proposed, permitting a rigorous estimation of the required number of slices under arbitrary excitations with harmonic content, without incurring excessive simulation time. This approach was benchmarked against numerical and experimental data, exhibiting robust performance when the maximum expected frequency and relative permeability are utilized in the calculation.

The analysis further demonstrates that the PMD model inherently accounts for the spatial inhomogeneity of the magnetic field, particularly under high-frequency and harmonic excitation, where pronounced attenuation and phase lag occur within the material. Consequently, this yields a superior time-domain estimation of iron losses with reduced experimental effort relative to Bertotti's analytical framework, as only the major hysteresis loop, electrical conductivity, and material dimensions are required.

Further research will focus on empirically validating the proposed heuristic for discretisation selection under more intricate excitation patterns, such as those encountered in PWM-driven systems. Additionally, the PMD model will be evaluated across a borader range of electrical steel materials and under a wider range of excitation waveforms. This will facilitate an assessment of the model's robustness and broaden its applicability to practical power electronic and electric machine applications.

6 References

[1] G. Mörée, M. Leijon: Iron Loss Models: A Review of Simplified Models of Magnetization Losses in Electrical Machines, Journal of Magnetism and Magnetic Materials, Vol. 609, November 2024, p. 172163.

[2] S. Steentjes, G. von Pfingsten, M. Hombitzer, K. Hameyer: Iron-Loss Model with Consideration of Minor Loops Applied to FE-Simulations of Electrical Machines, IEEE Transactions on Magnetics, Vol. 49, No. 7, July 2013, pp. 3945 – 3948.

[3] T. Taitoda, Y. Takahashi, K. Fujiwara: Iron Loss Estimation Method for a General Hysteresis Loop with Minor Loops, IEEE Transactions on Magnetics, Vol. 51, No. 11, November 2015, pp. 1 – 4.

[4] G. Bertotti: Hysteresis in Magnetism – for Physicists, Materials Scientists, and Engineers, Academic Press, San Diego, 1998.

[5] G. Mörée, M. Leijon: Review of Hysteresis Models for Magnetic Materials, Energies, Vol. 16, No. 9, May 2023, p. 3908.

[6] T. Chevalier, A. Kedous-Lebouc, B. Cornut, C. Cester: A New Dynamic Hysteresis Model for Electrical Steel Sheet, Physica B: Condensed Matter, Vol. 275, No. 1-3, January 2000, pp. 197 – 201.

[7] O. Messal, A.- T. Vo, M. Fassenet, P. Mas, S. Buffat, A. Kedous-Lebouc: Advanced Approach for Static Part of Loss-Surface Iron Loss Model, Journal of Magnetism and Magnetic Materials, Vol. 502, May 2020, p. 166401.

[8] A.- T. Vo, M. Fassenet, V. Préault, C. Espanet, A. Kedous-Lebouc: New Formulation of Loss-Surface Model for Accurate Iron Loss Modeling at Extreme Flux Density and Flux Variation: Experimental Analysis and Test on a High-Speed PMSM, Journal of Magnetism and Magnetic Materials, Vol. 563, December 2022, p. 169935.

[9] M. Petrun, S. Steentjes: Iron-Loss and Magnetization Dynamics in Non-Oriented Electrical Steel: 1-D Excitations Up to High Frequencies, IEEE Access, Vol. 8, January 2020, pp. 4568 – 4593.

[10] M. Petrun, S. Steentjes, K. Hameyer, D. Dolinar: 1-D Lamination Models for Calculating the Magnetization Dynamics in Non-Oriented Soft Magnetic Steel Sheets, IEEE Transactions on Magnetics, Vol. 52, No. 3, March 2016, pp. 1 – 4.

[11] M. Petrun, S. Steentjes, K. Hameyer, D. Dolinar: Magnetization Dynamics and Power Loss Calculation in NO Soft Magnetic Steel Sheets under Arbitrary Excitation, IEEE Transactions on Magnetics, Vol. 51, No. 1, January 2015, pp. 1 – 4.

[12] M. Petrun, V. Podlogar, S. Steentjes, K. Hameyer, D. Dolinar: A Parametric Magneto-Dynamic Model of Soft Magnetic Steel Sheets, IEEE Transactions on Magnetics, Vol. 50, No. 4, April 2014, pp. 1 – 4.

[13] L. Chen, Z. Zhang, T. Ben, H. Zhao: Dynamic Magnetic Hysteresis Modeling based on Improved Parametric Magneto-Dynamic Model, IEEE Transactions on Applied Superconductivity, Vol. 32, No. 6, September 2022, pp. 1 – 5.

[14] S. Steentjes, K. Hameyer, D. Dolinar, M. Petrun: Iron-Loss and Magnetic Hysteresis under Arbitrary Waveforms in NO Electrical Steel: A Comparative Study of Hysteresis Models, IEEE Transactions on Industrial Electronics, Vol. 64, No. 3, March 2017, pp. 2511 – 2521.

[15] J. Tellinen: A Simple Scalar Model for Magnetic Hysteresis, IEEE Transactions on Magnetics, Vol. 34, No. 4, July 1998, pp. 2200 – 2206.

[16] S. Yue, Y. Li, Q. Yang, X. Yu, C. Zhang: Comparative Analysis of Core Loss Calculation Methods for Magnetic Materials under Nonsinusoidal Excitations, IEEE Transactions on Magnetics, Vol. 54, No. 11, November 2018, pp. 1 – 5.

[17] H. Sun, Y. Li, Z. Lin, C. Zhang, S. Yue: Core Loss Separation Model under Square Voltage Considering DC Bias Excitation, AIP Advances, Vol. 10, No. 1, January 2020, p. 015229.

[18] G. Bertotti: General Properties of Power Losses in Soft Ferromagnetic Materials, IEEE Transactions on Magnetics, Vol. 24, No. 1, January 1988, pp. 621 – 630.